Atmospheric circulation features in the ACCESS model simulations for CMIP5: historical simulation and future projections

Harun A. Rashid, Anthony C. Hirst and Martin Dix
Centre for Australian Weather and Climate Research (CAWCR),
a partnership between CSIRO and the Bureau of Meteorology,
CSIRO Marine and Atmospheric Research, Aspendale, Australia

(Manuscript received July 2012; revised March 2013)

We evaluate the performance of two versions of the ACCESS model (1.0 and 1.3) in simulating both the historical (1979–2008) and projected (2071–2100) atmospheric circulations during, principally, the austral winter under two CMIP5 emission scenarios (RCP4.5 and RCP8.5). The model biases are estimated relative to two recent reanalysis datasets, while the projected circulation changes are assessed against the simulated historical circulations. Overall, both ACCESS models display model biases comparable in magnitude to other CMIP5 model biases. The most significant biases include the upper-tropospheric cold and polar warm biases, a westerly wind bias in the tropical upper troposphere and easterly wind biases in the southern and northern mid-latitudes, a narrower than observed Hadley circulation cell, a stronger Walker circulation cell, and drying (moistening) near the outer edges of the ascending (descending) branch of the Hadley cell. The projected circulation changes for the late 21st century in ACCESS simulations are largely similar to those found in the previous generation climate models including upper-tropospheric and polar warmings, a stronger subtropical jet, a poleward shifted mid-latitude jet, a deeper Hadley cell with its descending branch expanding poleward, and a weakened Walker circulation. However, our analysis also reveals a moderate intensification of the projected Hadley cell in the RCP4.5, but not the RCP8.5, simulations. Most of the projected changes are similar in ACCESS1.0 and ACCESS1.3, except that the Walker circulation change in ACCESS1.3 is essentially an eastward shift of its ascending branch to the east of the dateline, while that in ACCESS1.0 is an in-place weakening of the circulation.

Introduction

The atmosphere is the most important subsystem of the earth's climate system that directly affects the human life on a daily basis through its ever changing weather. The climate of a region, defined as the long-term statistics of weather, is locally determined by the many distinctive atmospheric circulation systems that constitute the global atmospheric circulation. Among the most prominent atmospheric circulation systems are the Hadley circulation, the Walker circulation, jet streams, monsoon circulations, and extratropical synoptic-scale cyclones. Scientists have long been studying the time-mean and time-varying characteristics of these circulation systems using observational analyses (e.g. Peixoto and Oort 1992), theoretical analyses (e.g. Gill 1982), and comprehensive numerical modelling (e.g. Washington and Parkinson 2005). In recent decades, global circulation models (GCMs) have emerged as an important tool for studying the atmospheric circulation systems, as well as other aspects of the climate system. The GCMs enable us to do numerical experiments to unravel the underlying mechanism of a circulation system or a climatic event, to predict weather and climate on a range of timescales, and to estimate the climate system response to imposed external forcings. An important precondition for the GCMs' utility for these purposes is, however, their ability to faithfully simulate the relevant characteristics of the climate system. This ability can only be gauged by a systematic evaluation of GCM simulations using available observations, a task which importantly also contributes to the further GCM development.

The Australian Community Climate and Earth System Simulator (ACCESS) is a coupled atmosphere–ocean–sea-

Corresponding author address: Harun Rashid, email: harun.rashid@csiro.au

ice model (hereafter, ACCESS-CM) developed by the Centre for Australian Weather and Climate Research (CAWCR) with contributions from the participating Australian universities (Bi et al. 2013). The ACCESS-CM is aimed at providing a comprehensive climate modelling capacity to Australian scientists. It has also been used to contribute to the CMIP5 project that, among other things, underpins the upcoming IPCC Fifth Assessment Report. Two versions of the ACCESS-CM, ACCESS1.0 and ACCESS1.3, were used to perform the core CMIP5 experiments requested by the PCMDI (Taylor et al. 2011, Dix et al. 2013). Both versions share essentially the same ocean and sea-ice component models, but use different atmospheric models (having significant differences in their cloud and land-surface parameterisation schemes; see the next section for details). In this paper, we evaluate the atmospheric circulation features over a recent historical period and document the projected circulation changes for the late 21st century using data from both ACCESS models for the historical experiment and two future emission scenario experiments. In particular, we examine the simulated Hadley and Walker circulations, the jet streams, as well as the vertical structure of air temperature and relative humidity under the historical and late 21st century conditions. Two recent atmospheric reanalysis datasets are utilised for the evaluation of the historical simulation, with the difference between the two reanalyses providing an estimate of the reanalysis uncertainty. The coupled simulations are also compared with the corresponding AMIP simulations in order to understand the possible sources of coupled model biases. The projected late 21st century simulations are assessed against the historical simulations. We limit the scope of this investigation to the southern hemisphere (SH) tropospheric circulation systems during winter, when the systems are most pronounced. An exception is the Walker circulation, which is strongest during the austral summer (e.g. Power and Smith 2007), and therefore is examined for this season. We leave out the discussion of the simulated surface climate, as this will be discussed elsewhere. For example, the global surface climate is described in Bi et al. (2013), Dix et al. (2013), Smith et al. (2013) and Watterson et al. (2013), the land-surface climate in Kowalczyk et al. (2013), while the interannual variability associated with the El Niño–Southern Oscillation (ENSO) events is documented in Rashid et al. (2013). Our main focus here is to document the fidelity of ACCESS-CM in simulating the key atmospheric circulation systems. However, where possible, we also compare ACCESS-CM results with the relevant published results from CMIP3 and CMIP5 models.

The paper is organised as follows. We first briefly describe the ACCESS-CM experiments and the reanalysis data used in this assessment, with pointers to more detailed descriptions. This is followed by a documentation of the model performance in simulating the historical atmospheric circulations. We then discuss the projected circulation changes for the late 21st century. Finally, some conclusions of this work are provided.

Model experiments and validation data

In this work, we use data from the ACCESS-CM simulations that have been contributed to the CMIP5 archive. The ACCESS model and the CMIP5 experiments have been documented in detail by Bi et al. (2013) and Dix et al. (2013), respectively. Here, we only highlight the major differences between the atmosphere components of ACCESS1.0 and ACCESS1.3. The atmosphere components are based on the UK Met Office Unified Model (version 7.3) and feature sophisticated parameterisations for unresolved physical processes involving radiation, clouds, aerosols, greenhouse gases, convection, gravity-wave drags, and the atmospheric boundary layer (Martin et al. 2011). In ACCESS1.0, the atmosphere model is configured to have the HadGEM2 climate configuration (Collins et al. 2008, Martin et al. 2011), whereas in ACCESS1.3 the atmospheric configuration is closely related to that of the Global Atmosphere version 1.0 (Hewitt et al. 2011, Walters et al. 2011). Thus, ACCESS1.3 uses a prognostic cloud scheme (Wilson et al. 2008) and ACCESS1.0 uses the diagnostic cloud scheme of Smith (1990). The other major difference is that ACCESS1.3 uses the CABLE land surface scheme (Kowalczyk et al. 2006, 2013), whereas ACCESS1.0 uses MOSES 2. In addition, the ACCESS1.3 version includes some further changes in the cloud, radiation, and boundary layer schemes as detailed in Bi et al. (2013). The ocean and sea-ice models used in both versions of ACCESS-CM are identical, except for a smaller critical Richardson number used in ACCESS1.0 ocean model (Rashid et al. 2013). The main impact of this change is to moderately increase ENSO strength through reduced mixings, and hence enhanced stratifications, in the upper equatorial thermocline. In addition, slightly different sea-ice albedos are used in the sea-ice models of ACCESS1.0 and ACCESS1.3 (Bi et al. 2013).

The ACCESS model simulations are driven by various anthropogenic climate forcings, arising from the changing concentrations of ozone, aerosols and the long-lived greenhouse gases (GHGs) in the atmosphere. The GHGs used are CO_2, CH_4, N_2O, CFC11, CFC12, CFC113, HCFC22, HCF125 and HFC134a. The included aerosol types are sulphate aerosols (SO_4), fossil fuel black carbon (FFBC), fossil fuel organic carbon (FFOC), biomass-burning aerosols (BB), biogenic secondary organic aerosols, sea-salt (SS), and mineral dust (DU). In addition, natural climate forcings due to variations in total solar irradiance (TSI) and the volcanic stratospheric aerosol concentration are used in the model simulations. In addition to the historical simulations, the same anthropogenic and natural forcings (for the relevant period) are used in the AMIP simulations. For the 21st century simulations, projected forcings from two of the CMIP5 emission scenarios, namely RCP4.5 and RCP8.5, are used. More details about the natural and anthropogenic climate forcings used in the ACCESS CMIP5 simulations may be found in Dix et al. (2013).

We use the 30-year period (1979–2008) for validating the historical simulations and the 30-year period (2071–2100) for calculating the late 21st century projected changes. The selected historical period facilitates comparison with modern reanalysis datasets, which normally begin at year 1979 to take advantage of available satellite data. Also, while some previous studies used 20 years of simulated data to estimate projected changes (e.g. Meehl et al. 2012), we have used a slightly longer 30-year period to reduce the sampling fluctuations of the computed time means. For the historical period we supplement the historical experiment data for 1979–2005 by three years (2006–2008) of simulation data from the RCP4.5 experiment. For the late 21st century circulation projections we use data from RCP4.5 and RCP8.5 scenario simulations, and compare the projections with the historical simulations to estimate the changes. For evaluation of the historical circulations, we use two new generation reanalysis datasets: the ERA-Interim reanalysis (Dee et al. 2011) and the NCEP climate forecast system reanalysis (CFSR) (Saha et al. 2010) for the period 1979–2008. To test the statistical significance of the estimated model biases and climate projections, we used a revised Student's *t*-test that takes into account the serial (or auto) correlation of climate time series (Zwiers and von Storch 1995). The serial correlations of the time series show spatial variation, therefore the threshold departure value that passes a particular significance level also varies over the spatial domain.

Simulation of historical atmospheric circulation features

Here, we compare the simulated zonal-mean air temperature, zonal wind, and meridional overturning stream function with available reanalysis data. This allows us to discuss the realism of the prominent atmospheric circulation systems, such as the jet streams and the Hadley Cell, in ACCESS simulations. These are examples of the zonally-symmetric circulation; we will also examine the simulated Walker circulation, an important example of the zonally-asymmetric circulation in the tropics. In addition to the results from reanalyses and coupled simulations, we also show the relevant AMIP experiment result. The latter is useful in understanding if a particular coupled model bias arises due to deficiencies in the atmospheric component model or in other component models (some of the model biases may also originate from errors associated with the coupling procedure).

Air temperatures

Figure 1 shows the zonal-mean air temperature from two reanalysis datasets (top row), two AMIP simulations (middle row) and two coupled simulations (bottom row) for the austral winter. The contours show the full zonal-mean values in the respective plots and the colour shadings show the differences from the values in the first plot (Fig. 1(a); ERA-Interim reanalysis). Therefore, the temperature differences in the top-right panel (Fig. 1(b)) give us an indication of the uncertainty among the two reanalysis datasets[1]. In general, the CFSR air temperatures are slightly colder than for ERA-Interim in the tropical middle-to-upper troposphere and over the South Pole; elsewhere they tend to be warmer (Fig. 1(b)). These differences between the reanalyses are, however, mostly not statistically significant (differences statistically significant at the 99 per cent level are stippled). Also, they are smaller than the biases in the AMIP (Fig. 1(c, d)) and coupled model simulations (Fig. 1(e, f)). Temperatures in ACCESS1.0 are colder throughout the troposphere (with a maximum cold bias of ~5 °C in the upper troposphere), except for a few regions in the polar mid-troposphere and the tropopause extending from the tropics to the northern hemisphere (NH) extratropics (Fig. 1(c, e)). In comparison, ACCESS1.3 shows somewhat warmer temperatures overall (Fig. 1(d, f)), with smaller (larger) cold (warm) biases. Also, the cold bias is somewhat stronger in coupled simulations than in AMIP simulations for both models. Interestingly, however, the ACCESS1.3 model shows a smaller bias in the coupled simulation than in the AMIP simulation (cf. Fig. 1(d, f)). Overall, the pattern of air temperature bias in the ACCESS models is similar to those in some other CMIP5 models (Martin et al. 2011, Watanabe et al. 2011) and to the multi-model mean bias seen in the CMIP3 climate models, with some differences in details (Reichler and Kim 2008b, their Fig. 4(b)). The latter implies that the ACCESS model bias is less than the individual model biases experienced by most of the CMIP3 models.

Jet streams

The zonal-mean zonal winds from reanalyses and model simulations are presented in Fig. 2. The main circulation features for the austral winter are the subtropical jet in the SH and the mid-latitude jet in the NH, with the former being the stronger with a peak magnitude of over 40 m s^{-1} in the upper troposphere (Fig. 2(a)). Compared to ERA-Interim, the jets in CFSR are slightly weaker; also, the westerlies over the SH high latitudes and the tropical easterlies tend to be stronger in this reanalysis (Fig. 2(b); see also Chelliah et al. 2011). These differences are, however, again smaller than the model biases. The main model bias, common to all simulations, is an overall westerly bias (of up to 6 m s^{-1}) over the tropics that makes the simulated tropical easterlies weaker compared to those in ERA-Interim. A zonal wind bias of comparable magnitude is also found in other CMIP5 models (Martin et al. 2011, Donner et al. 2011). There are significant zonal wind biases near the subtropical jet; the westerlies strengthen on the upper poleward side of the jet, which is part of an equatorward bias in the simulated stratospheric polar night jet (not shown). On the other hand, in all but the ACCESS1.3 AMIP simulation (Fig. 2(d)), the westerlies weaken (strengthen) on the lower poleward (equatorward) side of the jet (Fig. 2(c, e, f)). The latter gives

[1]Similar techniques were also used in the past to estimate observational or reanalysis uncertainties (Reichler and Kim 2008a).

Fig. 1. The latitude–pressure profiles of zonal-mean air temperatures (contours) from reanalyses ('observations') and ACCESS model simulations for 1979–2008. Also shown are the temperature differences (shades) between two reanalysis datasets as an estimate of the observational uncertainty, and between ACCESS simulations and a reanalysis as estimates of model biases. (a) ERA-Interim reanalysis, (b) CFSR reanalysis, (c) ACCESS1.0 AMIP simulation, (d) ACCESS1.3 AMIP simulation, (e) ACCESS1.0 historical simulation, and (f) ACCESS1.3 historical simulation. The contours represent the full temperature values, whereas the shades represent departures from ERA-Interim temperature. The stippling shows the statistically significant differences at the 99 per cent level from ERA-Interim. Values are shown for the southern winter (June–July–August) season, and the unit is °C.

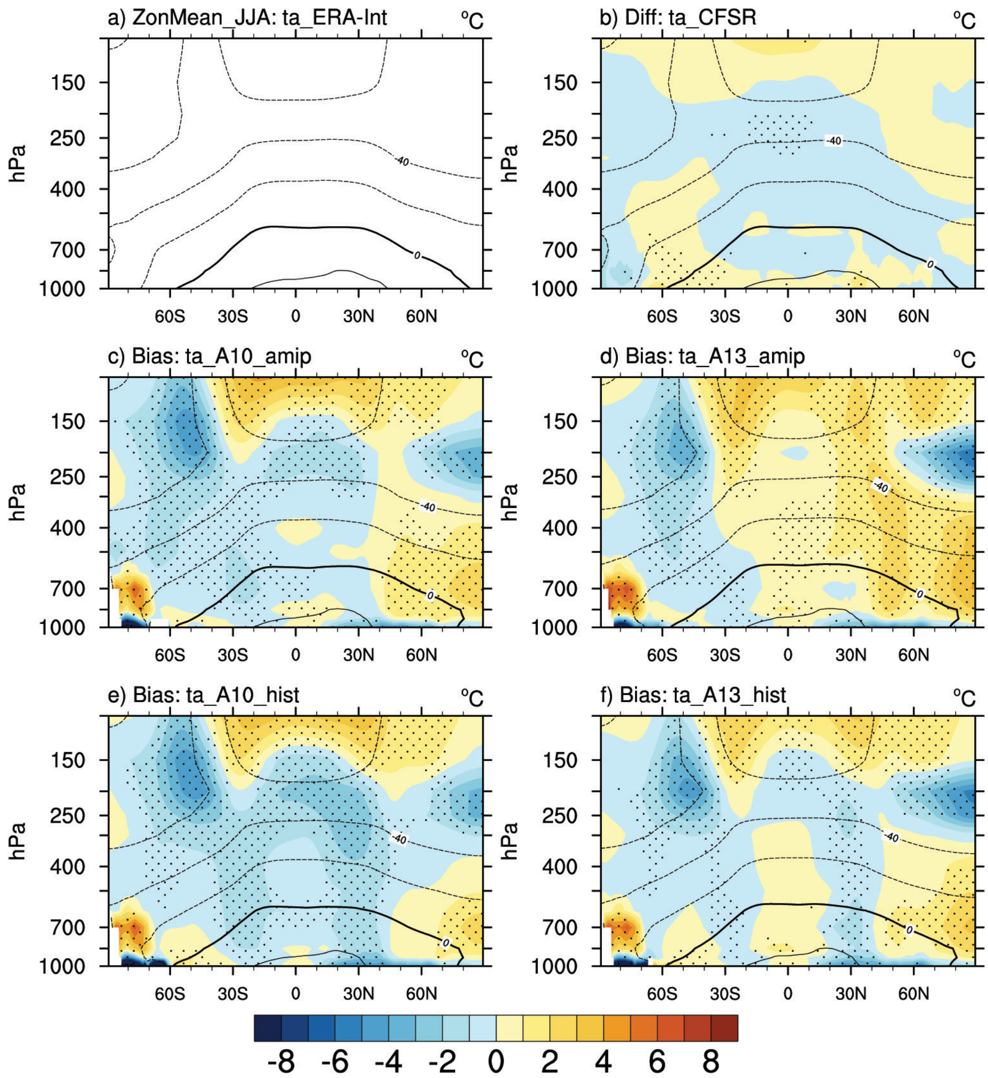

the impression of an equatorward shift in the simulated jet. However, an examination of the geographical (i.e. latitude–longitude) distribution of the upper-tropospheric zonal winds (not shown) reveals that this is not the case in any systematic sense zonally; the subtropical jet, which is most pronounced in the Australia–western Pacific sector, is simulated well by the models in terms of intensity and location. The largest contributions to the tropical westerly bias and the subtropical easterly bias, mentioned above, come from other regions of the tropics, e.g. the tropical north Pacific and the Africa–West Indian Ocean sector. In addition to these tropical–subtropical biases, there is a slight poleward shift of the NH midlatitude jet in simulations compared to ERA-Interim. The zonal wind biases in the tropics (extratropics) tend to be larger (smaller) in coupled simulations than in the respective AMIP simulations (Fig. 2(c–f)). The westerly bias in the NH tropical upper-troposphere and easterly bias in the SH subtropical upper troposphere appear to result from a narrower than observed Hadley cell simulated by the ACCESS coupled models (see the discussion of Fig. 3 below).

The Hadley and Ferrel cells

The Hadley circulation cells play an important role in shaping the global circulation of the atmosphere, for example, by transporting excess heat and momentum from the tropics to the extratropics (e.g. Holton 1992). This circulation system may be conveniently illustrated using the meridional overturning stream function, computed from the

Fig. 2. As in Fig. 1, except for the zonal-mean zonal wind (m s^{-1}). The solid (dashed) contours show the westerly (easterly) zonal winds.

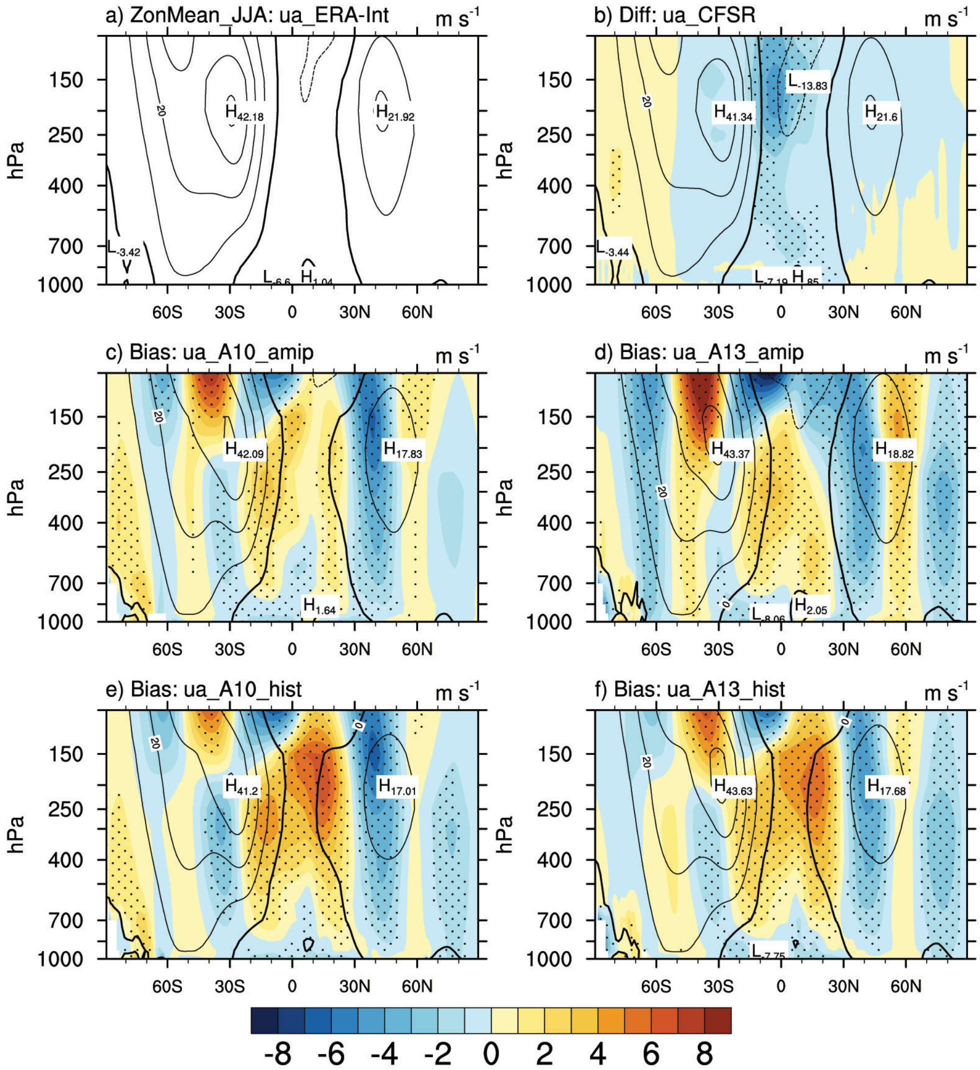

zonal-mean meridional wind (e.g. Waliser et al. 1999), which is displayed in Fig. 3 for reanalyses and model simulations. We again show results for the austral winter, when the Hadley cell is strongest in the SH (Fig. 3(a)). The NH cell is very weak in this season, as can be seen from the figure (see also Dima and Wallace 2003). In CFSR, the Hadley cell is stronger than in ERA-Interim, with the largest difference being in the ascending branch (Fig. 3(b)). This is consistent with the findings of Stachnik and Schumacher (2011), who discussed the differences in the Hadley cell strength, expansion and trend in a number of reanalyses, including ERA-Interim and CFSR. The model simulations show mixed results: in coupled simulations (Fig. 3(e, f)), the cell's vertical extent is shallower and the meridional width is narrower (due to contractions on both sides), but the cell is stronger (weaker) in ACCESS1.0 (ACCESS1.3) than observed. Also, the rising motions are concentrated in a narrower region than in observed due to their southward shifts. These biases are also clearly seen in the zonal-mean meridional and vertical winds (not shown). The AMIP simulations also show statistically significant biases (with a slightly stronger Hadley cell in both simulations), but these biases are smaller in magnitude than the differences between the two reanalyses (Fig. 3(b, c, d)). That the Hadley cell bias is different in coupled simulations to that in AMIP simulations indicates that the presence of equatorial SST biases in the coupled simulations (Bi et al. 2013, Rashid et al. 2013), and the resulting changes in the meridional SST gradient, may be partly responsible for the Hadley cell bias. For example, Gastineau et al. (2009) showed that the meridional structure of SST in their idealised experiments plays an important role in determining the Hadley cell response to global warming.

The tropical-subtropical zonal wind biases in the ACCESS coupled simulations (Fig. 2(e, f)) are consistent with a narrower than observed simulated Hadley cell. As the southward flowing upper branch of the Hadley cell in austral winter generates an easterly (westerly) acceleration of the zonal flow to the north (south) of the equator (due to

Fig. 3. As in Fig. 1, except for the meridional overturning stream function (10^{10} kg s^{-1}), depicting the Hadley cell. The dashed (solid) contours show counter-clockwise (clockwise) circulations.

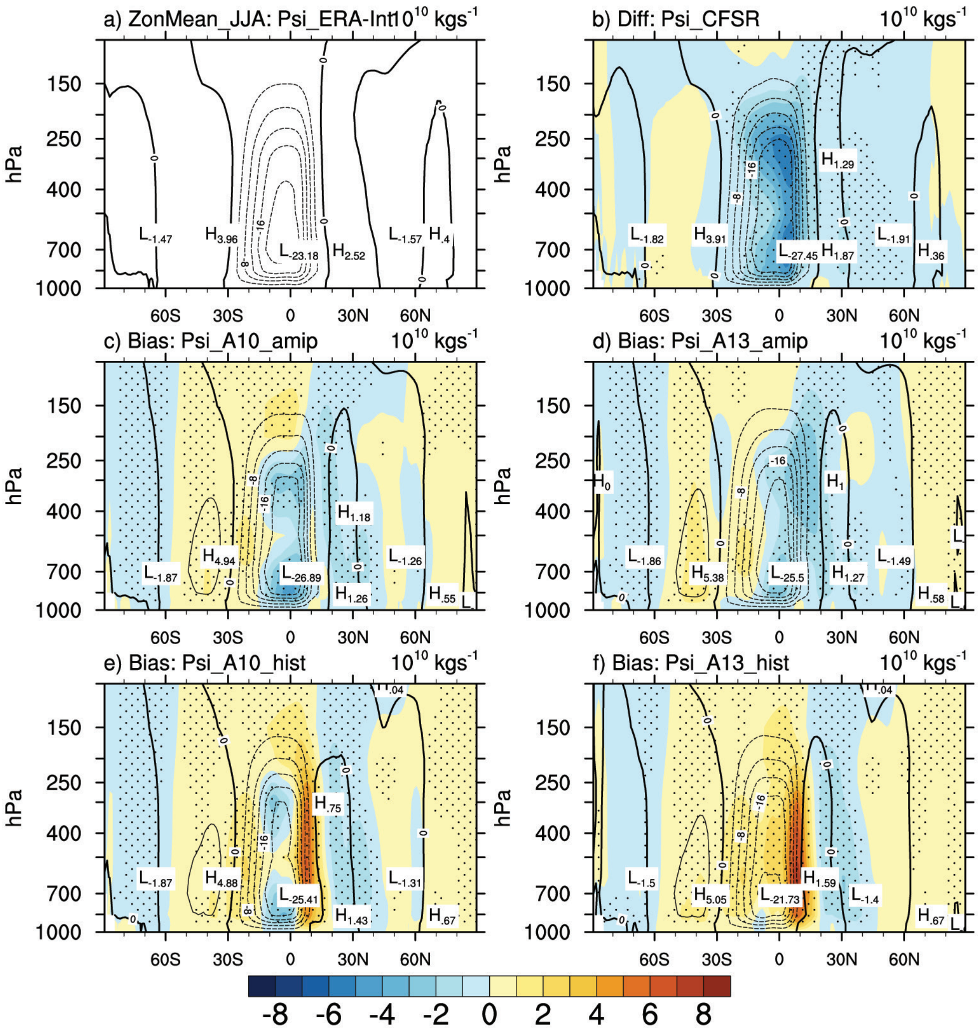

the Coriolis acceleration; see e.g. Fig. 11(c) in Dima et al. 2005), a narrower Hadley cell means that there are weaker than observed easterly (westerly) accelerations on the upper north (south) side of the simulated Hadley cell. This means a westerly zonal wind bias in the NH tropical upper troposphere and an easterly zonal wind bias in the SH subtropical upper troposphere (near the southern edge of the Hadley cell).

The thermally indirect Ferrel cell is much weaker than the Hadley cell, but nevertheless is an important part of the midlatitude circulation. The Ferrel cell can be seen in Fig. 3 between 30°S–60°S; this is slightly stronger in CFSR and in all model simulations than in ERA-Interim.

The Walker cell

The tropical zonal circulation comprises a number of east–west overturning cells with ascending motions over equatorial Africa, South America and the maritime continent and descending motions elsewhere (e.g. Holton 1992). The largest of these cells is the so-called Walker circulation cell that occurs in the Pacific sector and is most pronounced during the austral summer. Under normal conditions, this cell has its ascending branch in the western Pacific and the adjacent eastern Indian Ocean, while the descending branch is spread over the central and eastern Pacific. This is illustrated in Fig. 4, which shows the vector plots of divergent zonal wind and pressure vertical velocity at the equator for austral summer. Ascending motions of weaker magnitudes occur over the tropical African and South American continents. While ascent in ERA-Interim occurs over a broad longitude range around the Indonesian maritime continent (Fig. 4(a)), this occurs in CFSR over a more limited region (Fig. 4(b)). Otherwise, the differences between the two reanalyses are very small, except the ascending motion over equatorial Africa is largely absent in CFSR. In model simulations, the upward motions tend to be stronger than observed in the western Pacific. In AMIP simulations (Figs. 4(c, d)), there is a centre of large spurious upward motions over the western Indian Ocean, which is associated with an artificial rainfall maximum there (see Kowalczyk et al. 2013, their Fig. 8). This

Fig. 4. Vector plots of latitude-averaged (5°S–5°N) divergent zonal winds (U_{div}; m s^{-1}) and pressure vertical motions (ω; 0.02 Pa s^{-1}) from reanalyses and ACCESS model simulations for 1979–2008, depicting the Walker cell: (a) ERA-Interim, (b) CFSR, (c) ACCESS1.0 AMIP simulation, (d) ACCESS1.3 AMIP simulation, (e) ACCESS1.0 historical simulation, and (f) ACCESS1.3 historical simulation. The vectors in all panels represent the full values and a vector scale is shown in each panel. The contours in the first panel show the full values of U_{div}. Also shown are the U_{div} differences (shades) between two reanalysis datasets as an estimate of the observational uncertainty, and between ACCESS simulations and ERA-Interim as estimates of model biases. The stippling shows the U_{div} differences statistically significant at the 99 per cent level from ERA-Interim. Values are shown for the southern summer (December–January–February) season, when the Walker cell is most pronounced.

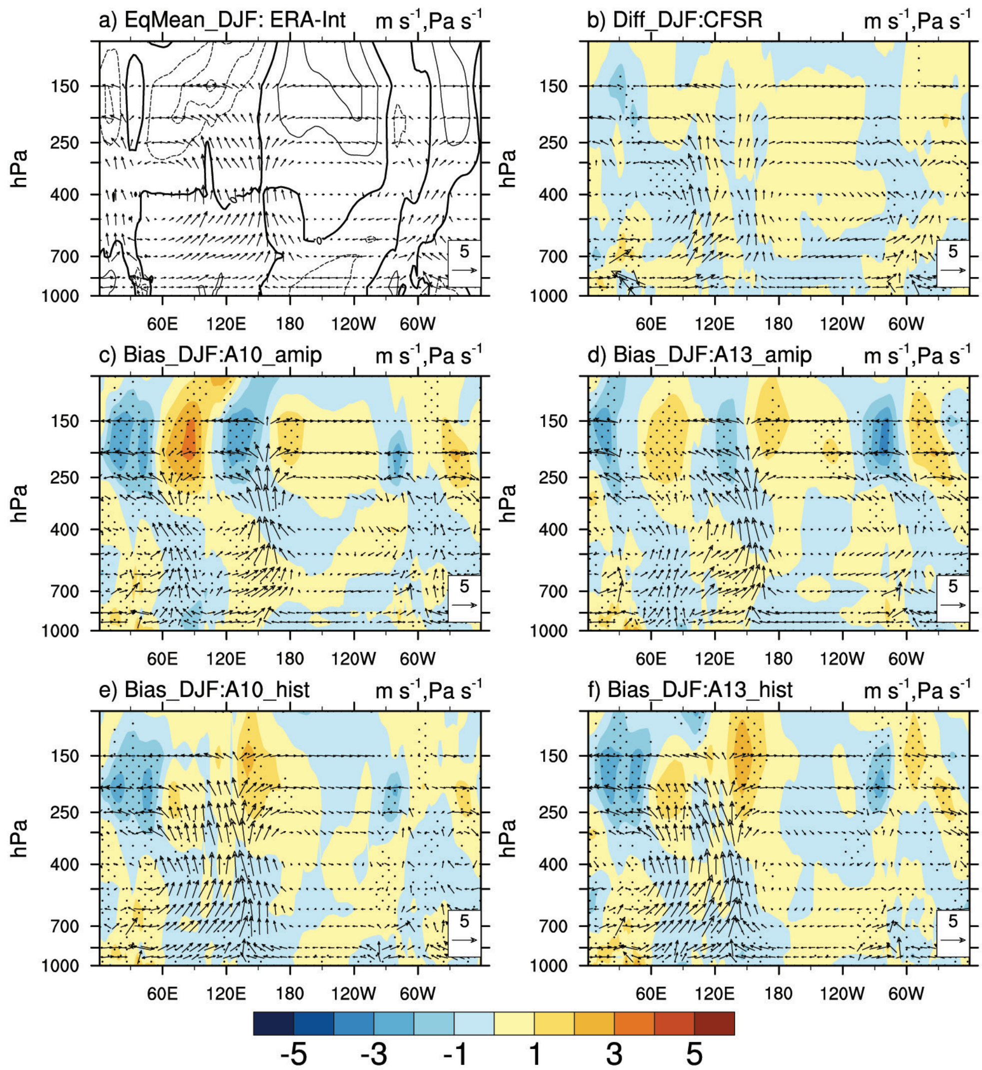

erroneous convection leads to a large divergent zonal wind bias in the upper troposphere. In coupled simulations (Fig. 4(e, f)), stronger than observed upward motions are found over the region extending from the western Pacific to the western Indian Ocean. In the latter region, the relatively large upward motions appear to be associated with the high spurious rainfall seen in that region in AMIP simulations (Kowalczyk et al. 2013). Also, the centre of ascending motion over equatorial Africa is largely absent in all model simulations as it is in CFSR.

Relative humidity

The pressure–latitude distribution of zonal-mean relative humidity is shown in Fig. 5 for the austral winter season. This is an important variable that may affect the model simulations of clouds (e.g. Sundqvist 1978), the associated radiative effects (e.g. Hartmann et al. 1992) and the water-vapour feedback (Pierrehumbert 1995, Sherwood et al. 2010). In ERA-Interim, the large values (in excess of 50 per cent) are confined in the lower troposphere over all latitudes, but extend throughout the troposphere in high latitudes and in a narrow region just north of the equator (Fig. 5(a)). The latter corresponds to the ascending branch of the Hadley cell during austral winter. Lower values of relative humidity, below 50 per cent, are found in the subtropical mid to upper troposphere that coincide with the descending branch of the Hadley cell. These reanalysis based results are consistent with the results derived from radiosonde observations

Fig. 5. As in Fig. 1, except for zonal mean relative humidity (per cent).

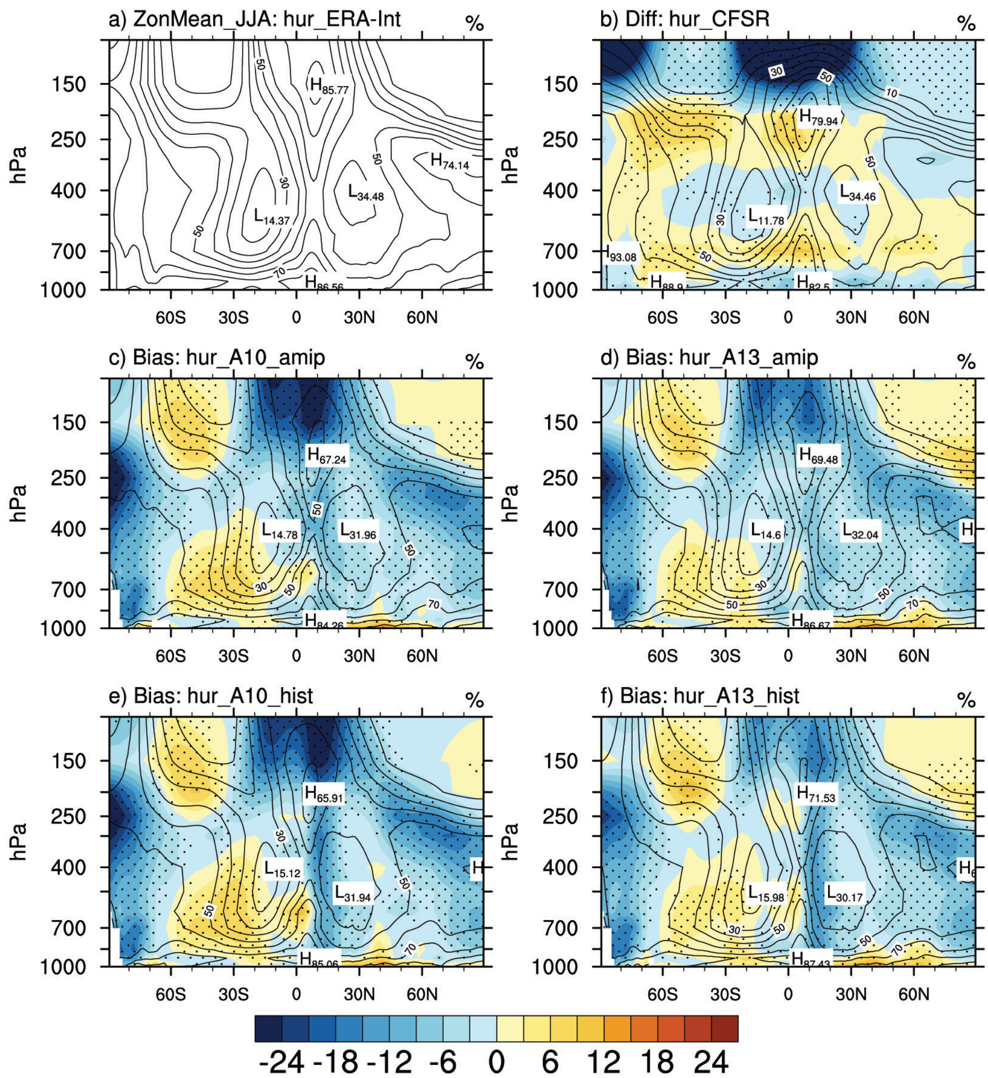

(Peixoto and Oort 1996). The relative humidity in CFSR shows only small differences from that in ERA-Interim throughout most of the troposphere (Fig. 5(b)); however, significantly lower values are seen in two isolated regions in the SH polar lower stratosphere and near the tropical tropopause. The latter appears to be due to a slightly shallower Hadley cell in CFSR (cf. Fig. 3(a, b)). The model simulated relative humidity is mostly lower than that in ERA-Interim, and the differences are larger in magnitude than the differences between two reanalyses in the troposphere. The lower values in the tropical troposphere may be explained by the equatorward contractions of the Hadley cell on the northern edge, while the contraction on the southern edge appears to explain the positive bias in the subtropical mid-troposphere. Relative humidity biases of comparable magnitudes are also found in other CMIP5 models (e.g. Watanabe et al. 2011).

In summary, the above analysis shows that the ACCESS model biases in the simulated atmospheric circulation features examined here are comparable to other CMIP5 model biases (e.g. Martin et al. 2011, Donner et al. 2011, Watanabe et al. 2011). Also, they are similar to the multi-model mean biases of the CMIP3 models (e.g. Reichler and Kim 2008b), implying that the ACCESS models show a better performance than the individual performance of the most previous generation climate models through reduced bias.

Projections for the late 21st century

We now assess the projected changes in above circulation features for the late 21st century (2071–2100) by comparing these with the simulated historical circulations (1979–2008).

Air temperatures

Figure 6 presents the pressure-latitude distribution of zonal-mean air temperatures from the historical experiment and from two future emission scenario experiments, RCP4.5 and RCP8.5, for austral winter. The top two panels show results from the ACCESS1.0 and ACCESS1.3 historical experiments for convenience of comparison. The middle (bottom) panels

Fig. 6. The latitude–pressure profiles of zonal-mean air temperatures (contours) for a recent historical period (1979–2008) and projections for the late 21st century (2071–2100) for the RCP4.5 and RCP8.5 scenarios. Also shown are the projected temperature changes (shades) with respect to the historical simulations. (a) ACCESS1.0 historical simulation, (b) ACCESS1.3 historical simulation, (c) ACCESS1.0 RCP4.5 simulation, (d) ACCESS1.3 RCP4.5 simulation, (e) ACCESS1.0 RCP8.5 simulation, and (f) ACCESS1.3 RCP8.5 simulation. The contours represent the full temperature values, whereas the shades represent departures of the RCP simulations from the historical simulations by the respective models. Statistically significant departures (at 99 per cent level) are stippled. Values are shown for the southern winter (June–July–August) season, and the unit is °C.

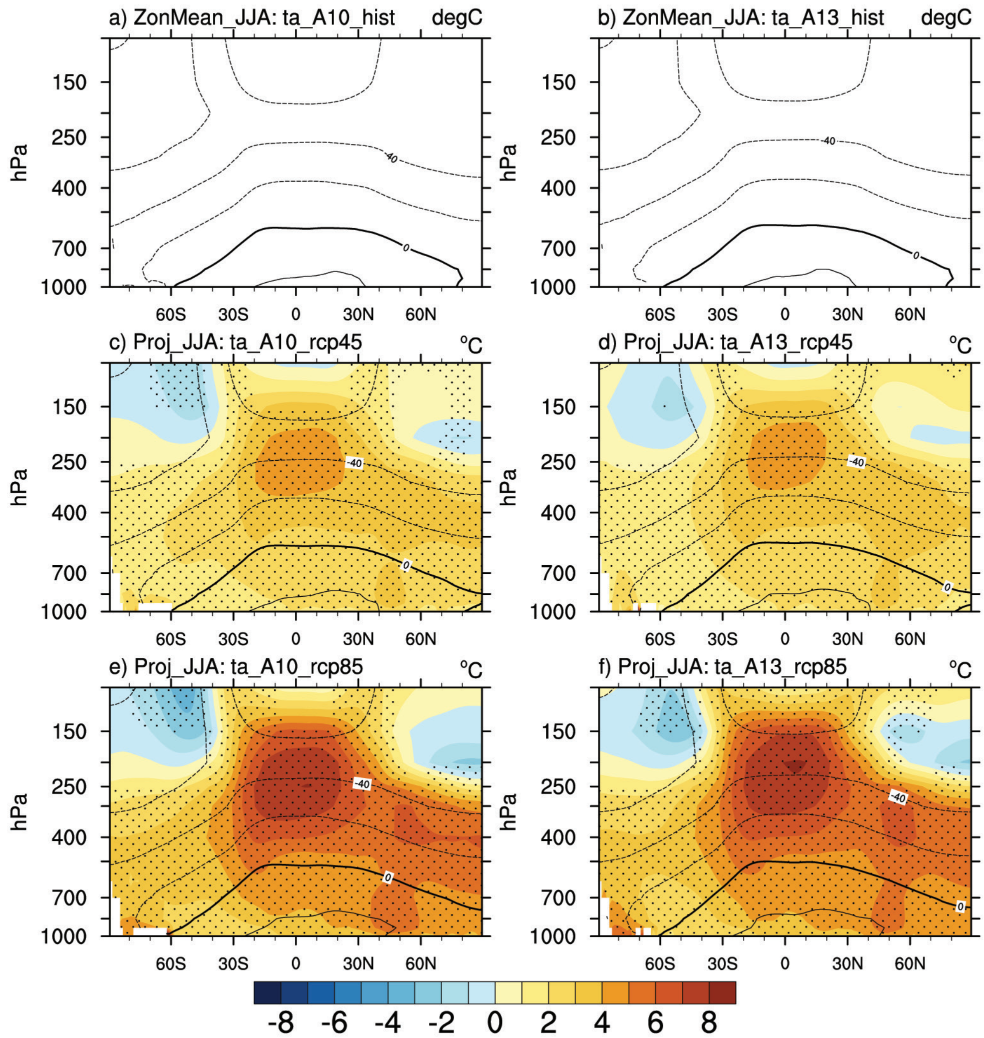

show the projected changes in RCP4.5 (RCP8.5) experiments, for ACCESS1.0 and ACCESS1.3, relative to the respective historical simulation. The changes for the RCP experiments (Fig. 6(c–f)) are shown in shades and the full values are shown by contours.

The projected temperature changes for late 21st century are a warming throughout the troposphere with the maximum warming occurring in the tropical upper troposphere. The maximum warming of around 4.5 °C in RCP4.5 is comparable to that in the A1B scenario for the CMIP3 multi-model means (Meehl et al. 2007), whereas the RCP8.5 warming (up to ~7 °C) is more comparable with the A2 scenario. As for CMIP3 model projections, the warming is larger in the NH than in the SH, and larger in the upper troposphere than at the surface. There are coolings in the extratropical lower stratospheres (and throughout the stratosphere; not shown). We note large meridional temperature gradients extending from the upper-troposphere to the stratosphere at midlatitudes, with the winter hemisphere gradient being stronger. The large-scale patterns of temperature change are similar in the RCP4.5 and RCP8.5 experiments, except that the latter experiment shows a larger change, as expected from its stronger external forcings (Meinshausen et al 2011). There appears to be no substantial difference between the temperature changes simulated by ACCESS1.0 and ACCESS1.3. Dix et al. (2013) draw a similar conclusion from an analysis of surface air temperatures. The pattern of temperature changes simulated by ACCESS models is also consistent with other CMIP5 models (e.g. Meehl et al. 2012).

The reliability of the model projection that the upper

Fig. 7. As in Fig. 6, except for the zonal mean zonal winds (m s^{-1}).

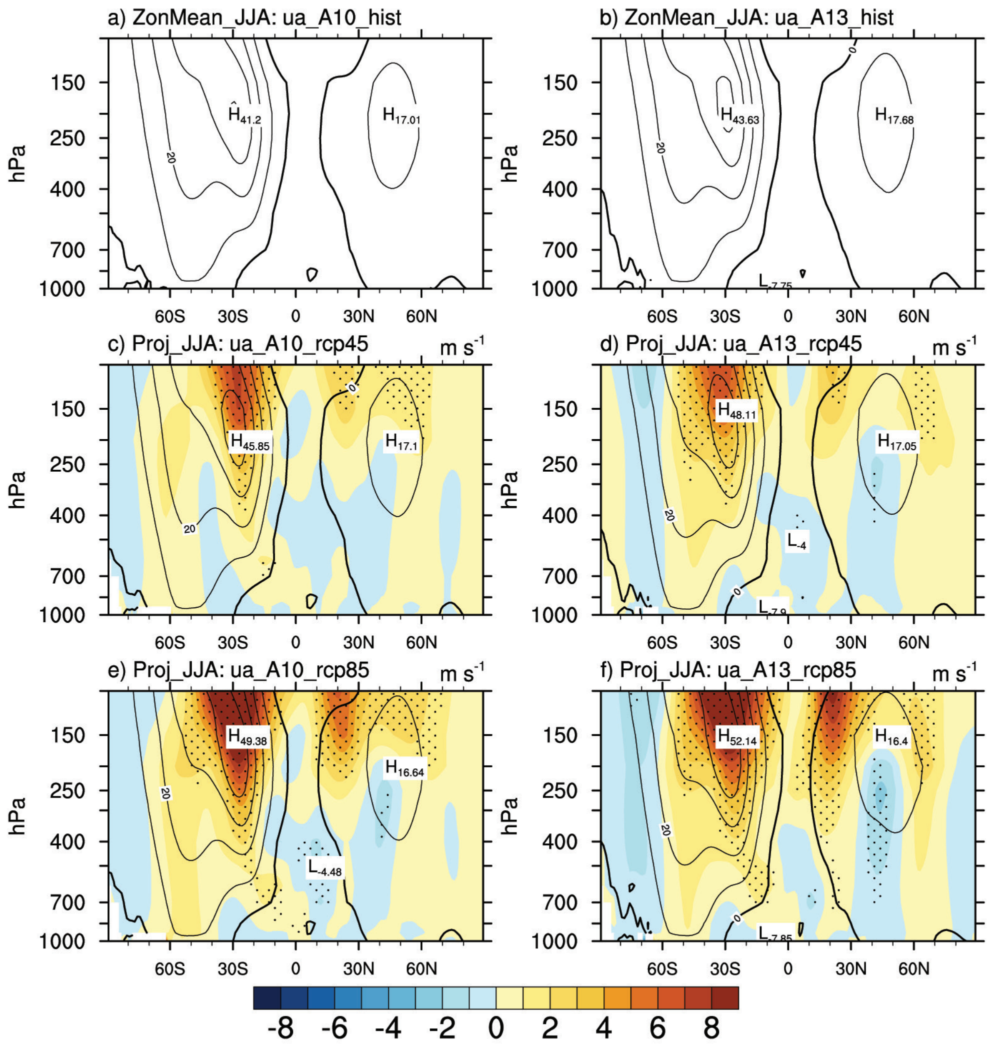

troposphere will warm more than the surface has been debated in the literature (see Thorne et al. 2011 for a review). The debate has been on the basis that some observational datasets do not show such an amplified upper-tropospheric warming over the historical period. However, many recent studies have suggested that the existing observational (radiosonde and satellite) temperature datasets suffer from time-dependent instrumental errors that hinder a reliable estimation of the observed upper-tropospheric temperature trends. Indeed, refined estimates of the latter using homogenised observational data, as well as alternative datasets, have removed the fundamental disagreement between the model projections and observations (Allen and Sherwood 2008, Thorne et al. 2011).

Jet streams

The historical values and their projected changes in the zonal-mean zonal winds are displayed in Fig. 7 for the austral winter. Also, Table 1 tabulates the meridional shifts and intensity changes of the principal hemispheric jets during both the austral winter and summer. The main tropospheric changes are a large increase in the subtropical jet strength (~8 m s^{-1} near the tropopause) and a moderate strengthening of the extratropical eddy-driven jet in the winter hemisphere (Fig. 7(c–f)). There is also a small northward shift of the subtropical jet found mainly in ACCESS1.0 simulations (Table 1.). The westerly (i.e. positive) wind change seen in the subtropical jet extends upward into the stratosphere, where the change is expressed as an equatorward shift of the polar night jet (not shown, but see Lorenz and DeWeaver 2007, Wu et al. 2012). This westerly wind change is related to the increased meridional temperature gradient seen in the same region (Fig. 6) through the thermal wind balance. In the NH, there is a poleward shift of the midlatitude jet (Table 1) and a westerly wind increase in the subtropical upper troposphere. Small easterly (i.e. negative) wind changes are also observed in some regions in Fig. 7(c–f), e.g. in the SH polar region and the tropical mid-troposphere, although the polar changes are too small to be statistically significant. During austral summer, the principal jet in each hemisphere strengthens and experiences a southward shift (Table 1). The

Fig. 8. As in Fig. 6, except for the meridional overturning stream function (10^{10} kg s^{-1}), depicting the Hadley cell. The dashed (solid) contours show counter-clockwise (clockwise) circulations.

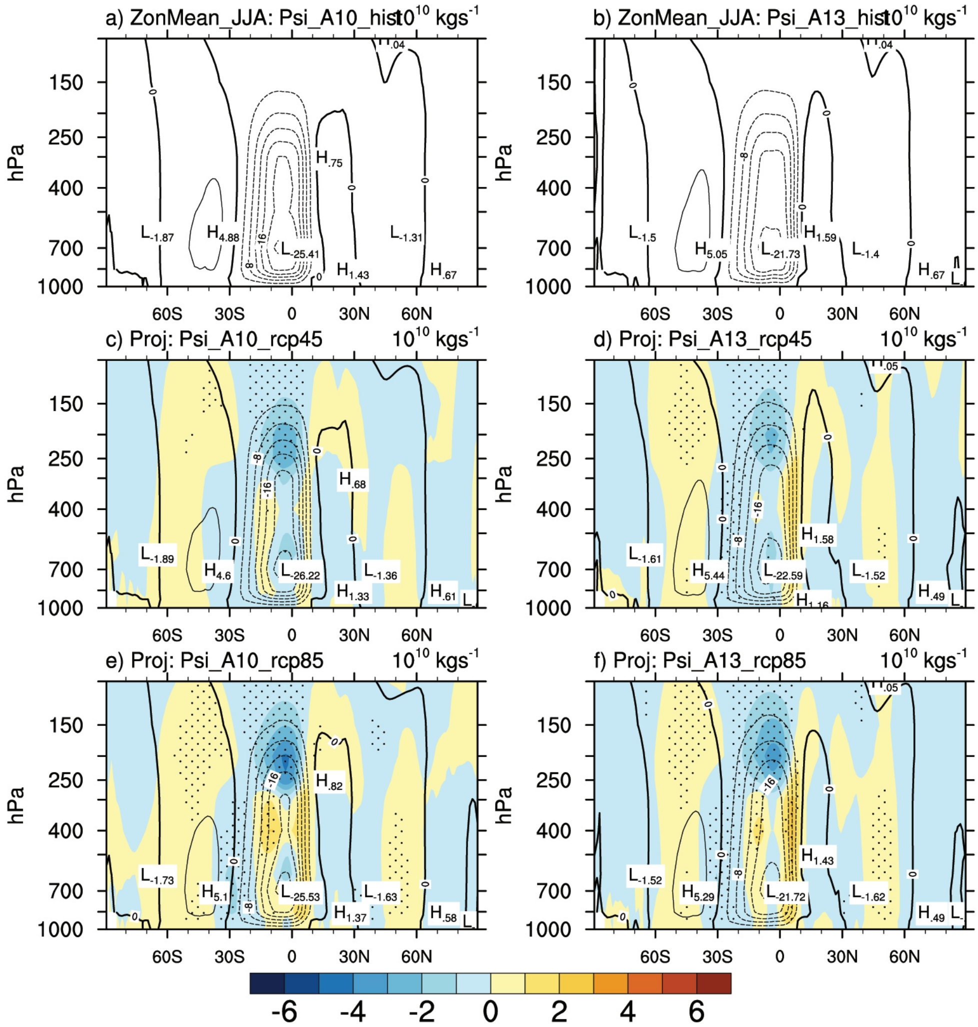

Table 1. Meridional shifts (deg. Lat) of the hemispheric principal jet streams in response to the anthropogenic global warming. The jet location is defined, separately for each hemisphere, as the latitude of the maximum zonal-mean zonal wind at 200 hPa. The jet shifts for the ACCESS1.0 and ACCESS1.3 RCP experiments (2071–2100) were calculated with respect to the respective historical experiments (1979–2008). Positive (negative) shift indicates a northward (southward) displacement of the jet maximum. The meridional shifts are measured as integer multiples of the models' meridional resolution (1.25°). The letters in parentheses indicate the changes of jet strength in the RCP experiments with respect to the respective historical experiments: S indicates strengthening, W indicates weakening, and U indicates unchanged.

	JJA				*DJF*			
Expts	*SH Jet shift (deg. Lat)*		*NH Jet shift (deg. Lat)*		*SH Jet shift (deg. Lat)*		*NH Jet shift (deg. Lat)*	
	A1.0	*A1.3*	*A1.0*	*A1.3*	*A1.0*	*A1.3*	*A1.0*	*A1.3*
RCP4.5	1.25 (S)	0 (S)	1.25 (U)	1.25 (W)	–2.5 (S)	0 (S)	0 (S)	–1.25 (S)
RCP8.5	1.25 (S)	0 (S)	1.25 (W)	0 (W)	–3.75 (S)	–1.25 (S)	–1.25 (S)	–1.25 (S)

Fig. 9. Vector plots of latitude-averaged (5°S–5°N) divergent zonal winds (U_{div}; m s^{-1}) and pressure vertical motions (ω; 0.02 Pa s^{-1}), showing the Walker circulation, for the historical period (1979–2008) and projections for the late 21st century (2071–2100) for the RCP4.5 and RCP8.5 scenarios: (a) ACCESS1.0 historical simulation, (b) ACCESS1.3 historical simulation, (c) ACCESS1.0 RCP4.5 simulation, (d) ACCESS1.3 RCP4.5 simulation, (e) ACCESS1.0 RCP8.5 simulation, and (f) ACCESS1.3 RCP8.5 simulation. The contours and vectors in the first two panels show the full values of U_{div} and the Walker circulation, respectively. The projected changes (c–f) in U_{div} (shades) and the Walker circulation (vectors) are estimated with respect to their historical values. The stippling shows the U_{div} changes statistically significant at the 99 per cent level from ERA-Interim. A scale for the vectors is provided in each plot; note the difference of vector scales in (a), (b) and (c–f). Values are shown for the southern summer (December–January–February) season, when the Walker cell is most pronounced.

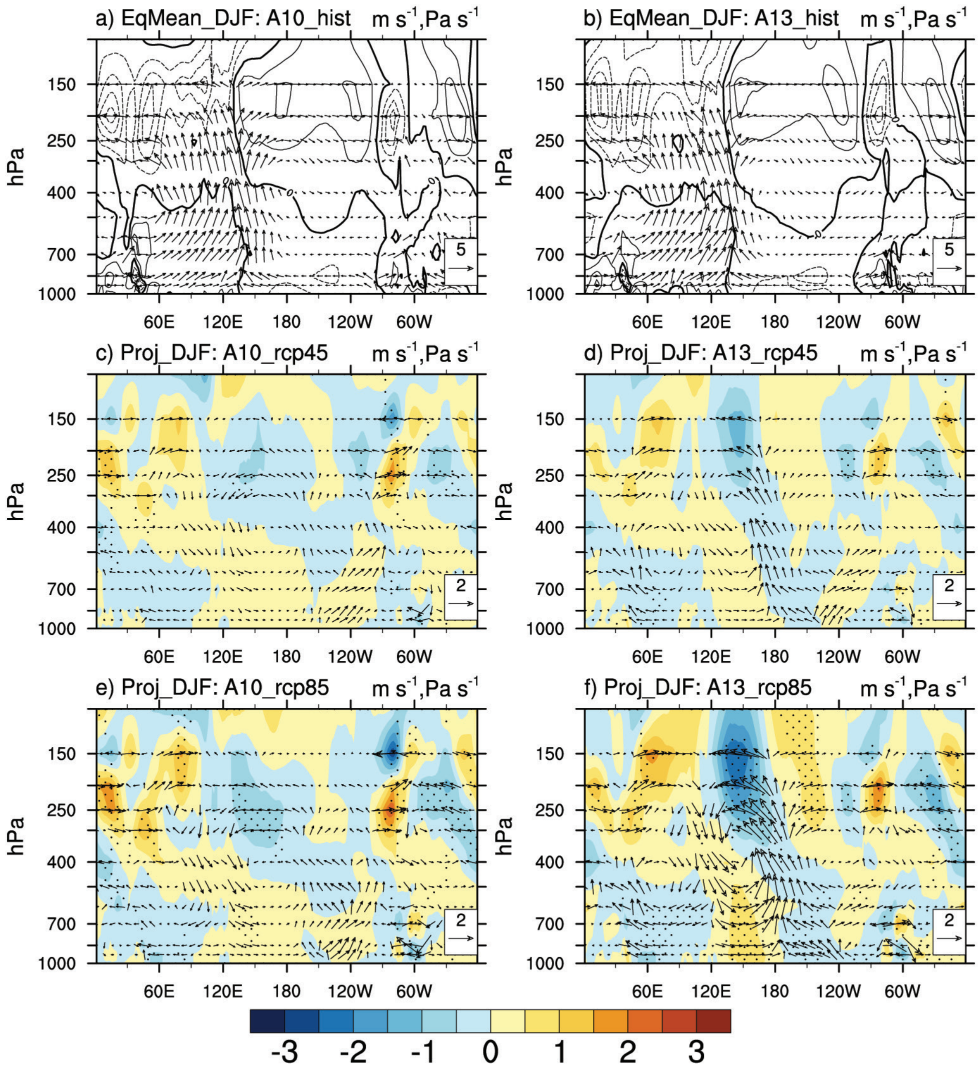

pattern and magnitude of the projected zonal wind changes in ACCESS models are comparable to the corresponding multi-model model mean projections of the CMIP3 models (Lorenz and DeWeaver 2007).

The Hadley and Ferrel cells

The Hadley and Ferrel cells and their changes under global warming are illustrated by the meridional overturning stream function, as before. The historical values and the projected changes of these cells are plotted in Fig. 8 for the austral winter. Also shown in Table 2 are the poleward expansions and intensity changes of the seasonal Hadley cell for both the austral winter and summer seasons. The main changes in the Hadley circulation include a deepening through vertical

Table 2. Poleward expansions of the seasonal Hadley Cell in response to the anthropogenic global warming. The numbers represent meridional shifts (in deg. Lat) of the zero-contour at 700 hPa designating the poleward edge of the Hadley Cell in the winter hemispheres. See the caption of Table 1 for other related information.

Expts	*JJA*		*DJF*	
	A1.0	*A1.3*	*A1.0*	*A1.3*
RCP4.5	0 (S)	–1.25 (S)	0 (W)	1.25 (W)
RCP8.5	–1.25 (U)	–1.25 (U)	1.25 (W)	1.25 (W)

Fig. 10. As in Fig. 6, except for zonal mean relative humidity (per cent).

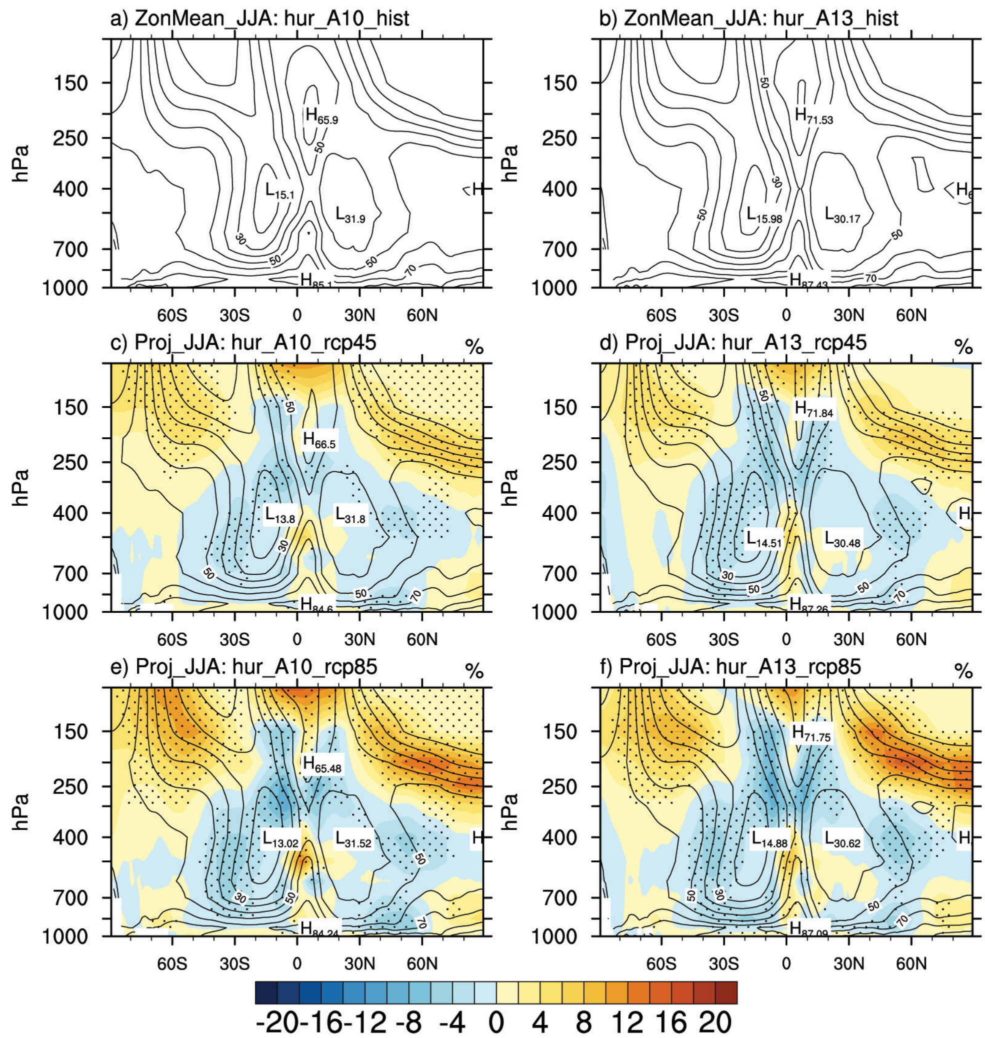

extension of the cell, a poleward expansion at the southern edge, and an equatorward contraction on the northern edge (Fig. 8(c–f)). The extent of the poleward expansions, in degrees latitude, is shown in Table 2 for the SH Hadley cell in austral winter and the NH Hadley cell in austral summer. All the RCP experiments show the poleward expansion (except for the ACCESS1.0 RCP4.5 experiment) in addition, the RCP4.5 experiments show a strengthening of the cell (i.e. the minimum value of the stream function decreases further; see Fig. 8(c, d) and Table 2) during the austral winter. During the austral summer, however, the Hadley cell weakens in all the RCP experiments. The poleward expansion of the Hadley cell has been found to be a robust feature in analyses of historical records (Stachnik and Schumacher 2011, Hu and Fu 2007, Fu et al. 2006) and of climate change projections by CMIP3 class models (Gastineau et al. 2008, Mitas and Clement 2006). However, the small intensification of the SH Hadley cell found in RCP4.5 experiments is not consistent with the moderate weakening trend projected by most CMIP3 models (Gastineau et al. 2008), though it is consistent with observed intensification over the historical period (Stachnik and Schumacher 2011). Surprisingly, the SH Hadley cell intensification is non-existent in RCP8.5 simulations (Fig. 8(e, f)) in both models. Also, the projected deepening of the Hadley cell in ACCESS simulations is in accord with the observed and model predicted increase of the tropopause height under anthropogenic forcings (e.g. Kushner et al. 2001; Santer et al. 2003). Apart from these changes in the Hadley cell, there is no apparent change found for the eddy-driven Ferrel cell, except for a hint of a poleward displacement.

The Walker cell

The tropical zonal circulation change under global warming has been extensively studied using coupled model simulations from the CMIP3 archive (e.g. Held and Soden 2006, Vecchi and Soden 2007). The CMIP3 simulations generally show a weakening of the Walker circulation during the 21st century, although the sign of the forced change for the 20th century is ambiguous according to recent observational and modelling work (Power and Kociuba 2011, Meng et al. 2012).

The projected zonal circulation changes in ACCESS model simulations are presented in Fig. 9. While we analysed all the other circulation features for the austral winter, we assessed the Walker circulation for the austral summer, when this circulation system is the strongest. The pattern of changes is somewhat different between ACCESS1.0 and ACCESS1.3: in the former, the ascending motions around the West Pacific maritime continent appear to weaken in response to global warming (Fig. 9(c, e)). While a similar weakening of the ascending motions is also seen in the ACCESS1.3 projections, there is also a significant strengthening to the east of this region, over the central Pacific (Fig. 9(d, f)). This strengthening results from an eastward expansion of the ascending motion in ACCESS1.3 RCP simulations, as an examination of the full projected zonal circulation fields reveals (not shown). In fact, the ascending motions in this model expand both eastward and westward, occupying the sector between 60°E to 180° longitudes, accompanied by a weakening in the middle, around 120°E longitude. This is manifested in the projected anomaly fields (Fig. 9(d, f)) as anomalous upward motions near 60°E and 180° and downward motions near 120°E. Therefore, the Walker circulation change in ACCESS1.3 is characterised by an eastward shift of its ascending branch. On the other hand, the projected change in ACCESS1.0 simulation is a weakening of the Walker circulation, expressed as anomalous downward (upward) motion in the region of historical upward (downward) motions in the tropical west (east) Pacific.

Relative humidity

The relative humidity changes during the late 21st century are presented in Fig. 10 for the austral winter. The changes are mostly negative, except for the tropopause region, tropical mid-troposphere and the lower half of the NH polar troposphere. The strongest drying occurs in the tropical upper troposphere and over the subtropics (extratropics) of the SH (NH), constituting a horseshoe-shaped pattern. This drying pattern has also been observed previously in CMIP3 models (Richter and Xie 2008, Sherwood et al. 2010, Wright et al. 2010), and has been attributed to various changes associated with global warming, such as the poleward expansion of the Hadley cell and increase in tropopause height. These latter changes are also clearly seen in ACCESS model simulations (cf. Figs 6 and 8), and are likely to be responsible for the relative humidity changes. The moistening (drying) in the tropical tropopause (upper troposphere) appears to be due to an upward shift of the detrainment level associated with a deepening Hadley cell under global warming. The moistening in the tropical mid-troposphere is consistent with a stronger Hadley circulation and larger evaporation from the tropical oceans (not shown) projected by the ACCESS models. Also, the lower-tropospheric moistening in the NH polar region may be associated with the excess evaporation that results from the northern summer sea-ice retreat (Uotila et al. 2013) associated with large warmings found in that region (Fig. 6).

Discussion and conclusions

In this paper, we investigate the realism of the historical (1979–2008) atmospheric circulations and discuss their projected changes in the late 21st century (2071–2100) under the anthropogenic emission scenarios, as simulated by the two versions of the ACCESS coupled model, ACCESS1.0 and ACCESS1.3. We restrict our discussion mostly to the austral wintertime tropospheric circulation features above the surface, as the results concerning the simulated surface climate will be presented elsewhere. The coupled model biases in some prominent circulation systems have been estimated using two recent reanalyses (ERA-Interim and CFSR). The main biases are: (i) the upper-tropospheric cold and polar warm biases, (ii) a westerly wind bias in the tropical upper troposphere and easterly wind biases in the southern and northern midlatitudes, (iii) a narrower than observed Hadley circulation cell, (iv) a stronger Walker circulation cell, and (v) drying (moistening) near the outer edges of the ascending (descending) branch of the Hadley cell, resulting from the latter being narrower in the model simulations. These biases are found, for the most part, to be comparable to the multi-model mean biases of CMIP3 models, suggesting that the performance of ACCESS models is better than the individual performance of most previous generation models. We also found the ACCESS model performance to be comparable to some other CMIP5 models, for which the relevant evaluation results have been published (e.g. Martin et al. 2011, Donner et al. 2011, Watanabe et al. 2011). Our assessment is consistent with a quantitative, skill-score based evaluation of 25 CMIP5 models that places the ACCESS models among the upper performing CMIP5 models for key surface variables (Watterson et al. 2013).

The projected changes for the late 21st century according to the RCP4.5 and RCP8.5 emission scenarios are assessed against the simulated historical circulations. The main results are: (i) tropospheric warmings with the maximum being in the upper-troposphere and the NH polar region, (ii) a strengthening of the wintertime subtropical jet and a poleward shift of the summertime midlatitude jet, (iii) a deepened Hadley cell with poleward expansion, (iv) a weakening of the Walker cell, and (v) a pattern of relative humidity change that is mostly consistent with the changes in the Hadley cell. The SH Hadley cell also shows moderate intensification in the RCP4.5 case, and this differs from the projections of the previous generation models. While the Hadley cell intensifies in the RCP4.5 simulations, this intensification is not seen in the RCP8.5 simulations, despite the latter simulations having larger GHG forcings. Recent simulations suggest that increasing aerosols may weaken the simulated Hadley cell in austral winter (Rotstayn et al. 2012); thus decreasing aerosols, as in the RCP emission scenarios, may strengthen it. Therefore, a plausible explanation for the different Hadley cell responses may be that, in the RCP4.5 experiments, the Hadley cell is primarily responding to the decreasing aerosols, with the weakening effect of the GHGs being secondary. On the other hand, the GHG forcings are stronger in the RCP8.5 experiments than in RCP4.5 experiments, and the strengthening of the Hadley cell due to decreasing aerosols is largely being balanced by the weakening due to a stronger increase in GHGs. We also find that the projected Walker cell changes in the ACCESS models are different: in ACCESS1.0 (ACCESS1.3) the Walker cell weakening results from an in-place weakening (eastward shift) of this cell.

The main features of the projected changes are qualitatively similar to those found in previous generation climate models and also in some CMIP5 models for which the relevant results are published. This suggests that the projected changes from both ACCESS models and other CMIP5 and CMIP3 models are robust for the features examined here, despite the fact that there are substantial differences (e.g. in parameterisations, resolutions, and forcing scenarios) between the current and previous generation of climate models. It is, however, likely that models will differ in their projections for other features, such as rainfall, and for regional climate change, given these features' higher sensitivity to model deficiencies. This situation can only be improved through continuing development of the models' parameterisation schemes and by increasing their spatio-temporal resolutions, accompanied by critical evaluations of climate model simulations of past and future climates.

Acknowledgments

We are grateful to the reviewers and the Associate Editor for providing insightful comments on the paper. This work has been undertaken as part of the Australian Climate Change Science Program, funded jointly by the Department of Climate Change and Energy Efficiency, the Bureau of Meteorology and CSIRO. The simulations were performed at the NCI National Facility at the Australian National University. We thank Dr. Ian Watterson for his comments on an early draft of this paper, and we thank the members of the coupled modelling team at CAWCR for their roles leading to the ACCESS-CM CMIP5 contributions. The authors thank Dr. Lawrence Rikus and Mr. Ben Hu for downloading and maintaining an archive of reanalysis data, some of which are used in this work.

References

Allen, R.J., and Sherwood, S.C. 2008. Warming maximum in the tropical upper troposphere deduced from thermal winds. *Nat. Geosci, 1,* 399–403.

Bi, D., Dix, M., Marsland, S.J., O'Farrell, S., Rashid, H.A., Uotila, P., Hirst, A.C., Kowalczyk, E., Golebiewski, M., Sullivan, A., Yan, H., Hanna, N., Franklin, C., Sun, Z., Vohralik, P., Watterson, I., Zhou, X., Fiedler, R., Collier, M., Ma, Y., Noonan, J., Stevens, L., Uhe, P., Zhu, H., Hill, R., Harris, C., Griffies, S. and Puri, K. 2013. The ACCESS Coupled Model: Description, Control Climate and Preliminary Validation. *Aust. Met. Oceanog. J.*, 63, 41–64.

Chelliah, M., Ebisuzaki, W., Weaver, S. and Kumar, A. 2011. Evaluating the tropospheric variability in National Centers for Environmental Prediction's climate forecast system reanalysis. *J. Geophys. Res., 116,* D17107, doi:10.1029/2011JD015707.

Collins, W.J., Bellouin, N., Doutriaux-Boucher, M., Gedney, N., Hinton, T., Jones, C.D., Liddicoat, S., Martin, G., O'Connor, F., Rae, J., Senior, C., Totterdell, I., Woodward, S., Reichler, T. and Kim, J. 2008. *Evaluation of the HadGEM2 model.* Met Office Hadley Centre Technical Note no. HCTN 74, available from Met Office, FitzRoy Road, Exeter EX1 3PB. http://www.metoffice.gov.uk/publications/HCTN/index.html

Dee, D.P., Uppala, S.M., Simmons, A.J., Berrisford, P., Poli, P., Kobayashi, S., Andrae, U., Balmaseda, M.A., Balsamo, G., Bauer, P., Bechtold, P., Beljaars, A.C.M., van de Berg, L., Bidlot, J., Bormann, N., Delsol, C., Dragani, R., Fuentes, M., Geer, A.J., Haimberger, L., Healy, S.B., Hersbach, H., Hólm, E.V., Isaksen, L., Kållberg, P., Köhler, M., Matricardi, M., McNally, A.P., Monge-Sanz, B.M., Morcrette, J.-J., Park, B.-K., Peubey, C., de Rosnay, P., Tavolato, C., Thépaut, J.-N. and Vitart, F. 2011. The ERA-Interim reanalysis: configuration and performance of the data assimilation system. *Q. J. R. Meteorol. Soc., 137,* 553–97.

Dima, I.M., and Wallace, J.M. 2003. On the Seasonality of the Hadley Cell. *J. Atmos. Sci., 60,* 1522–7.

Dima, I.M., Wallace, J.M. and Kraucunas, I. 2005. Tropical Zonal Momentum Balance in the NCEP Reanalyses. *J. Atmos. Sci., 62,* 2499–513.

Dix, M., Vohralik, P., Bi, D., Rashid, H.A., Marsland, S.J., O'Farrell, S., Uotila, P., Hirst, A.C., Kowalczyk, E., Sullivan, A., Yan, H., Franklin, C., Sun, Z., Watterson, I., Collier, M., Noonan, J., Rotstayn, L., Stevens, L., Uhe P. and Puri, K. 2013. The ACCESS Coupled Model: Documentation of core CMIP5 simulations and initial results. *Aust. Met. Oceanog. J.*, 63, 83–99.

Donner, L.J., Wyman, B.L., Hemler, R.S., Horowitz, L.W., Ming, Y., Zhao, M., Golaz, J.-C., Ginoux, P., Lin, S.-J., Schwarzkopf, M.D., Austin, J., Alaka, G., Cooke, W.F., Delworth, T.L., Freidenreich, S.M., Gordon, C.T., Griffies, S.M., Held, I.M., Hurlin, W.J., Klein, S.A., Knutson, T.R., Langenhorst, A.R., Lee, H.-C., Lin, Y., Magi, B.I., Malyshev, S.L., Milly, P.C.D., Naik, V., Nath, M.J., Pincus, R., Ploshay, J.J., Ramaswamy, V., Seman, C.J., Shevliakova, E., Sirutis, J.J., Stern, W.F., Stouffer, R.J., Wilson, R.J., Winton, M., Wittenberg, A.T. and Zeng, F. 2011. The dynamical core, physical parameterizations, and basic simulation characteristics of the atmospheric component of the GFDL global coupled model CM3. *J. Clim., 24,* 3484–519.

Fu, Q., Johanson, C.M., Wallace, J.M. and Reichler, T. 2006. Enhanced midlatitude tropospheric warming in satellite measurements. *Science, 312,* 1179, doi:10.1126/science.1125566.

Gastineau, G., Le Treut, H. and Li, L. 2008. Hadley circulation changes under global warming conditions indicated by coupled climate models. *Tellus, 60A,* 863–84.

Gastineau, G., Li, L. and Treut, H.L. 2009. The Hadley and Walker Circulation Changes in Global Warming Conditions Described by Idealized Atmospheric Simulations. *J. Clim., 22,* 3993–4013. doi: http://dx.doi.org/10.1175/2009JCLI2794.1

Gill, A. E. 1982. *Atmosphere–Ocean Dynamics.* Academic Press, 662 pp.

Hartmann, D.L., Ockert-Bell, M.E. and Michelsen, M.L. 1992: The effect of cloud type on Earth's energy balance: Global analysis. *J. Clim., 5,* 1281–304.

Held, I. M. and Soden, B.J. 2006. Robust responses of the hydrological cycle to global warming. *J. Clim., 19,* 5686–99.

Hewitt, H.T., D. Copsey, I.D. Culverwell, C.M. Harris, R.S.R. Hill, A.B. Keen, A.J. McLaren, and Hunke. 2011. Design and implementation of the infrastructure of HadGEM3: the next-generation Met Office climate modelling system. *Geosci. Model Dev., 4,* 223–53, doi:10.5194/gmd-4-223-2011.

Holton, J.R. 1992. *An Introduction to Dynamic Meteorology*. 3d ed. Academic Press, 511 pp.

Hu, Y. and Fu, Q. 2007. Observed poleward expansion of the Hadley circulation since 1979. *Atmos. Chem. Phys., 7,* 5229–36, doi:10.5194/ acp-7-5229-2007.

Kowalczyk, E.A., Y.P. Wang, R.M. Law, H.L. Davies, J.L. McGregor and G. Abramowitz. 2006. The CSIRO Atmosphere Biosphere Land Exchange (CABLE) model for use in climate models and as an offline model. CSIRO Marine and Atmospheric Research paper 013, www.cmar.csiro.au/e-print/open/kowalczykea_2006a.pdf

Kowalczyk, E.A., L. Stevens, R.M. Law, M. Dix, Y.P. Wang, I.N. Harman, K. Hayens, J. Srbinovsky, B. Pak, and T. Zhien. 2013. The land surface model component of ACCESS: description and impact on the simulated surface climatology. *Aust. Met. Oceanog. J.,* 63, 65–82.

Kushner, P.J., Held, I.M. and Delworth, T.L. 2001. Southern Hemisphere atmospheric circulation response to global warming. *J. Clim., 14,* 2238–49.

Lorenz, D.J. and DeWeaver, E.T. 2007. Tropopause height and zonal wind response to global warming in the IPCC scenario integrations. *J. Geophys. Res., 112,* D10119, doi:10.1029/2006JD008087.

HadGEM2 Development Team: Martin, G.M., Bellouin, N., Collins, W.J., Culverwell, I.D., Halloran, P.R., Hardiman, S.C., Hinton, T.J., Jones, C.D., McDonald, R.E., McLaren, A.J., O'Connor, F.M., Roberts, M.J., Rodriguez, J.M., Woodward, S., Best, M.J., Brooks, M.E., Brown, A.R., Butchart, N., Dear- den, C., Derbyshire, S.H., Dharssi, I., Doutriaux-Boucher, M., Edwards, J.M., Falloon, P.D., Gedney, N., Gray, L.J., Hewitt, H.T., Hobson, M., Huddleston, M.R., Hughes, J., Ineson, S., Ingram, W.J., James, P.M., Johns, T.C., Johnson, C.E., Jones, A., Jones, C.P., Joshi, M.M., Keen, A.B., Liddicoat, S., Lock, A.P., Maidens, A.V., Manners, J.C., Milton, S.F., Rae, J.G.L., Ridley, J.K., Sellar, A., Senior, C. A., Totterdell, I.J., Verhoef, A., Vidale, P.L., and Wiltshire, A., 2011: The HadGEM2 family of Met Office Unified Model climate configurations. *Geosci. Model Dev., 4,* 723–57, doi:10.5194/gmd-4-723-2011.

Meehl, G.A. and coauthors. 2007. Global climate projections. *Climate Change 2007: The Physical Science Basis,* S. Solomon et al. Eds., Cambridge University Press, 746–845.

Meehl, G.A., W.M. Washington, J.M. Arblaster, A. Hu, H. Teng, C. Tebaldi, B.N. Sanderson, J.-F. Lamarque, A. Conley, W.G. Strand, J.B. White. 2012. Climate System Response to External Forcings and Climate Change Projections in CCSM4. *J. Clim., 25,* 3661–83.

Meinshausen, M., Smith, S.J., Calvin, K.V., Daniel, J.S., Kainuma, M.L.T., Lamarque, J.-F., Matsumoto, K., Montzka, S.A., Raper, S.C.B., Riahi, K., Thomson, A.M., Velders, G.J.M. and van Vuuren, D. 2011: The RCP greenhouse gas concentrations and their extension from 1765 to 2300. *Clim. Change, 109,* 213–41, doi:10.1007/s10584-011-0156-z.

Meng, Q., Latif, M., Park, W., Keenlyside, N.S., Semenov, V.A., Martin, T. 2012. Twentieth century Walker Circulation change: data analysis and model experiments. *Clim. Dyn., 38,* 1757–73.

Mitas, C.M., and Clement, A. 2005. Has the Hadley cell been strengthening in recent decades? *Geophys. Res. Lett., 32,* L03809, doi:10.1029/2004GL021765.

Peixoto, J.P., and Oort, A.H. 1992. *Physics of Climate*. American Institute of Physics, 520 pp.

Peixoto, J.P., and Oort, A.H. 1996. The climatology of relative humidity in the atmosphere. *J. Clim., 9,* 3443–63. doi:10.1175/15200442(1996)009<3443: TCORHI>2.0.CO;2.

Pierrehumbert, R. 1995. Thermostats, radiator fins, and the local runaway greenhouse. *J. Atmos. Sci., 52,* 1784–806. doi:10.1175/1520-0469(1995)052<1784:TRFATL> 2.0.CO;2.

Power, S.B. and Smith, I.N. 2007. Weakening of the Walker Circulation and apparent dominance of El Niño both reach record levels, but has ENSO really changed? *Geophys. Res. Lett., 34,* L18702, doi:10.1029/2007GL030854.

Power, S.B. and Kociuba, G. 2011. What Caused the Observed Twentieth-Century Weakening of the Walker Circulation? *J. Clim., 24,* 6501–14. doi: http://dx.doi.org/10.1175/2011JCLI4101.1

Rashid, H.A., Sullivan, A., Hirst, A.C., Bi, D., Zhou, X. and Marsland, S.J. 2013. Evaluation of El Niño–Southern Oscillation in the ACCESS coupled model simulations for CMIP5. *Aust. Met. Oceanogr. J.,* 63, 161–80.

Reichler, T. and Kim, J. 2008a. Uncertainties in the climate mean state of global observations, reanalyses, and the GFDL climate model. *J. Geophys. Res., 113,* D05106, doi:10.1029/2007JD009278.

Reichler, T. and Kim, J. 2008b. How well do coupled models simulate today's climate. *Bull. Am. Meteorol. Soc., 89,* 303–11.

Richter, I. and Xie, S.-P. 2008. Muted precipitation increase in global warming simulations: A surface evaporation perspective. *J. Geophys. Res., 113,* D24118, doi:10.1029/2008JD010561.

Rotstayn, L.D., Jeffrey, S.J., Collier, M.A., Dravitzki, S.M., Hirst, A.C., Syktus, J.I., and Wong, K.K. 2012. Aerosol- and greenhouse gas-induced changes in summer rainfall and circulation in the Australasian region: a study using single-forcing climate simulations. *Atmos. Chem. Phys., 12,* 6377–404, doi:10.5194/acp-12-6377-2012.

Saha S., S. Moorthi, H.-L. Pan, X. Wu, J. Wang, S. Nadiga, P. Tripp, R. Kistler, J. Woollen, D. Behringer, H. Liu, D. Stokes, R. Grumbine, G. Gayno, J. Wang, Y.-T. Hou, H.-Y. Chuang, H.-M.H. Juang, J. Sela, M. Iredell, R. Treadon, D. Kleist, P.V. Delst, D. Keyser, J. Derber, M. Ek, J. Meng, H. Wei, R. Yang, S. Lord, H. van den Dool, A. Kumar, W. Wang, C. Long, M. Chelliah, Y. Xue, B. Huang, J.-K. Schemm, W. Ebisuzaki, R. Lin, P. Xie, M. Chen, S. Zhou, W. Higgins, C.-Z. Zou, Q. Liu, Y. Chen, Y. Han, L. Cucurull, R.W. Reynolds, G. Rutledge, M. Goldberg. 2010. The NCEP climate forecast system reanalysis. *Bull. Am. Meteorol. Soc. 91,* 1015–57.

Santer, B.J., M.F. Wehner, T.M.L. Wigley, R. Sausen, G.A. Meehl, K.E. Taylor, C. Ammann, J. Arblaster, W.M. Washington, J.S. Boyle, and W. Brüggemann. 2003. Contributions of anthropogenic and natural forcing to recent tropopause height changes. *Science, 301,* 479–83.

Sherwood, S.C., W. Ingram, Y. Tsushima, M. Satoh, M. Roberts, P.L. Vidale, and P.A. O'Gorman. 2010. Relative humidity changes in a warmer climate. *J. Geophys. Res., 115,* D09104, doi:10.1029/ 2009JD012585.

Smith, I., Syktus, J., Rotstayn, L. and Jeffrey, S. 2013. The relative performance of Australian CMIP5 models based on rainfall and ENSO metrics. *Aust. Met. Oceanogr. J., 63,* 205–212.

Stachnik, J.P., and Schumacher, C. 2011. A comparison of the Hadley circulation in modern reanalyses. *J. Geophys. Res., 116,* D22102, doi:10.1029/2011JD016677.

Sundqvist, H. 1978. A parameterization scheme for non-convective condensation including prediction of cloud water content. *Q. J. R. Meteorol. Soc., 104,* 677–90.

Thorne, P.W., Lanzante, J.R., Peterson, T.C., Seidel, D.J., and Shine, K.P. 2011. Tropospheric temperature trends: History of an ongoing controversy. *WIRCC, 2,* 66–88, doi:10.1002/wcc.80.

Uotila, P., O'Farrell, S., Marsland, S.J., and Bi, D. 2013. The sea-ice performance of the Australian climate models participating in the CMIP5. *Aust. Met. Oceanogr. J.,* 63, 121–43.

Vecchi, G.A. and Soden, B.J. 2007. Global warming and the weakening of the tropical circulation. *J. Clim., 20,* 4316–40.

Waliser, D.E., Shi, Z., and Lanzante, J.R. 1999. The Hadley circulation: Assessing NCEP/NCAR reanalysis and sparse in-situ estimates. *Clim. Dyn., 15,* 719–35.

Walters, D.N., Best, M.J., Bushell, A.C., Copsey, D., Edwards, J.M., Falloon, P.D., Harris, C.M., Lock, A.P., Manners, J.C., Morcrette, C.J., Roberts, M.J., Stratton, R.A., Webster, S., Wilkinson, J.M., Willett, M.R., Boutle, I.A., Earnshaw, P.D., Hill, P.G., MacLachlan, C., Martin, G.M., Moufouma-Okia, W., Palmer, M.D., Petch, J.C., Rooney, G.G., Scaife, A.A., and Williams, K.D. 2011. The Met Office Unified Model Global Atmosphere 3.0/3.1 and JULES Global Land 3.0/3.1 configurations. *Geosci. Model Dev., 4,* 919–41, doi:10.5194/gmd-4-919-2011.

Washington, W.M. and Parkinson, C.L. 2005. *An Introduction to Three-Dimensional Climate Modeling*. University Science Books, 2nd ed., 353 pp.

Watanabe, S., Hajima, T., Sudo, K., Nagashima, T., Takemura, T., Okajima, H., Nozawa, T., Kawase, H., Abe, M., Yokohata, T., Ise, T., Sato, H., Kato, E., Takata, K., Emori, S. and Kawamiya, M. 2011. MIROC-ESM 2010 model description and basic results of CMIP5-20c3m experiments. *Geosci. Model Dev., 4,* 845–72, doi:10.5194/gmd-4-845-2011.

Watterson, I.G., Hirst A.C., and Rotstayn, L.D. 2013. A skill-score based evaluation of simulated Australian climate. *Aust. Met. Oceanogr. J.,* 63, 181–90.

Wright, J., Sobel, A., and Galewsky, J. 2010. Diagnosis of zonal mean relative humidity changes in a warmer climate. *J. Clim., 23,* 4556–69.

Wu, Y., Seager, R., Ting, M., Naik, N., and Shaw. T.A. 2012. Atmospheric Circulation Response to an Instantaneous Doubling of Carbon Dioxide. Part I: Model Experiments and Transient Thermal Response in the Troposphere. *J. Clim., 25,* 2862–79.

Zwiers, F.W., and von Storch, H. 1995. Taking serial correlation into account in tests of the mean. *J. Clim., 8,* 336–51.